Power-law decay of doubly ionized ethylene

K. Takahashi, K. Yokokawa, A. Mizumura, J. Matsumoto, and H. Shiromaru*
Department of Chemistry, Tokyo Metropolitan University, Hachioji, Tokyo 192-0397, Japan

H. Kumar
Department of Physics and Astrophysics, University of Delhi, Delhi 110007, India

P. Bhatt and C. P. Safvan
Inter-University Accelerator Centre, Aruna Asaf Ali Marg, New Delhi 110067, India

(Received 11 September 2018; published 17 December 2018)

Delayed dissociation of doubly ionized ethylene, produced by collisions of highly charged ions, was studied at low and medium collision energies. Position-sensitive time-of-flight measurements of all the recoil fragments, triggered by detection of a charge-selected scattered ion, or emitted electrons, allowed us to identify ionic dissociation processes accompanied by delayed processes. We found that the delayed dissociation processes are well described by the power-law decay, rather than the exponential decay.

DOI: 10.1103/PhysRevA.98.062708

I. INTRODUCTION

Delayed molecular processes of ionization, electron detachment, dissociation, and photon emission have been intensively studied for a long time, and they still attract keen attention in molecular science. For example, such processes involve information on the internal temperature and how it goes down radiatively [1]. Power-law decay of the product yields, rather than exponential decay, is a hot topic in ion storage studies [2–5]. For the ionic dissociation (charge separation) of doubly ionized molecules as well, delayed processes have been found for various dications: from diatomic dications (CO^{2+} [6–9], SH^{2+} [10], $N_2{}^{2+}$ [9], HCl^{2+} [11]) to doubly ionized large molecules (brominated derivative of uracil [12] and $C_{60}{}^{2+}$ [13], for example).

Deprotonation of doubly ionized ethylene, $C_2H_4{}^{2+} \rightarrow C_2H_3{}^{+} + H^{+}$, accompanies a delayed process with a long lifetime. The nondissociative dicationic channel in which the lifetime of the dication is longer than its flight time to the detector is also identified [14]. The lifetime of the deprotonation channel is measured by femtosecond laser irradiation studies [15,16]. In the time-of-flight (TOF) coincidence map, a long tail of delayed ionic dissociation connects the coordinates of [TOF1 = TOF(H^{+}), TOF2 = TOF($C_2H_3{}^{+}$), prompt deprotonation] and [TOF1 = TOF2 = TOF($C_2H_4{}^{2+}$), nondissociative dication], reflecting its long lifetime. The TOF information is converted to the survival time of $C_2H_4{}^{2+}$. Ionization by 4.5 fs laser shows that the decay profile with the survival time is, for the slow component, well fitted by a single exponential function with a $1/e$ lifetime of about 498 ns [15]. Specific vibronic states responsible for the delayed deprotonation, which can be directly populated by the laser irradiation, are identified based on theoretical calculations. The authors of [15] also proposed an alternative explanation of over-the-barrier dissociation, in which the vibrational energies in all the vibrational modes play a role. Jochim *et al.* adapted a two-term exponential function to the results obtained by 23 fs laser irradiation, and the best fit is obtained by 269 and and 956 ns for fast and slow components, respectively [16]. They pointed out that the difference might be not essential because the single exponential fit of their data gives nearly the same lifetime (491 ns) as that by Larimian *et al.* Meanwhile, it should be noted that the ionization scheme depends on the pulse duration. The difference between 4.5 and 23 fs is not small and the population of the vibronic states can be different [17].

In the present study, double ionization of ethylene by low- and medium-energy collisions of highly charged atomic ions and subsequent ionic dissociation was observed. By multihit position-sensitive TOF (PSTOF) measurements, survival time of the metastable dications was obtained. In general, the ionization scheme depends on the collision energy. It is due to multiple electron capture in the low-energy region where the velocity (or the energy per unit mass) is fairly lower than 1 a.u. (or an energy of about 25 keV/u), while ionization also plays a role at higher energy. We will examine whether the dissociation scheme of the delayed deprotonation is common for all, or dependent on the ionization processes.

II. EXPERIMENTS

Low-energy collision experiments were performed at a beamline of the 14.25 GHz Electron Cyclotron Resonance (ECR) ion source at Tokyo Metropolitan University (TMU-ECRIS) [18]. Ar^{n+} ($n = 4, 8$) extracted from the ECR ion source was introduced to the collision chamber, which was constructed from two existing apparatuses in order to carry out capture in selective experiments [19,20]. Since the details of the apparatus are shown in elsewhere [21], a brief description

*Corresponding author: shiromaru-haruo@tmu.ac.jp

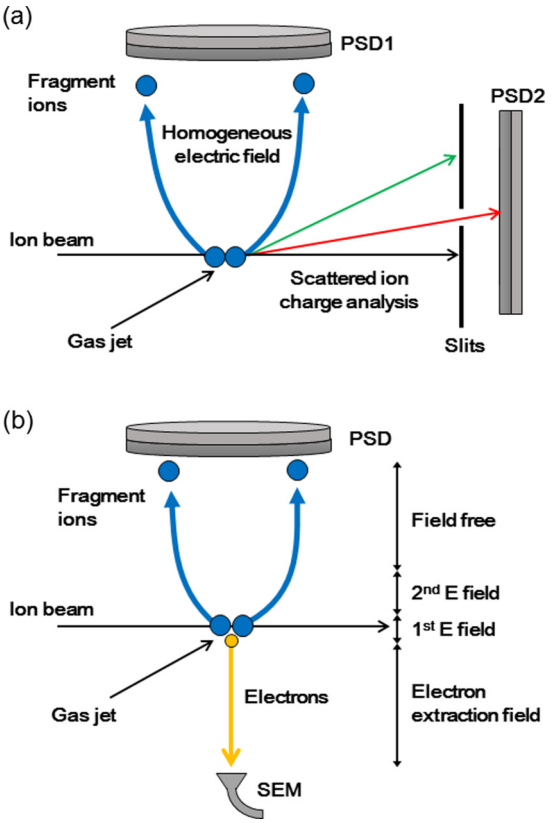

FIG. 1. (a) Schematic view of the apparatus for low-energy collision (TMU). The scattered ions are deflected according to the charge states, and the charge-dispersed ions are selected with the slit. The recoil and scattered ions are detected with PSD1 and PSD2, respectively. (b) Schematic view of the apparatus for medium-energy collision (IUAC). The recoil ions are detected by a PSD, and the emitted electrons accelerated to the opposite direction are detected by an electron multiplier (SEM).

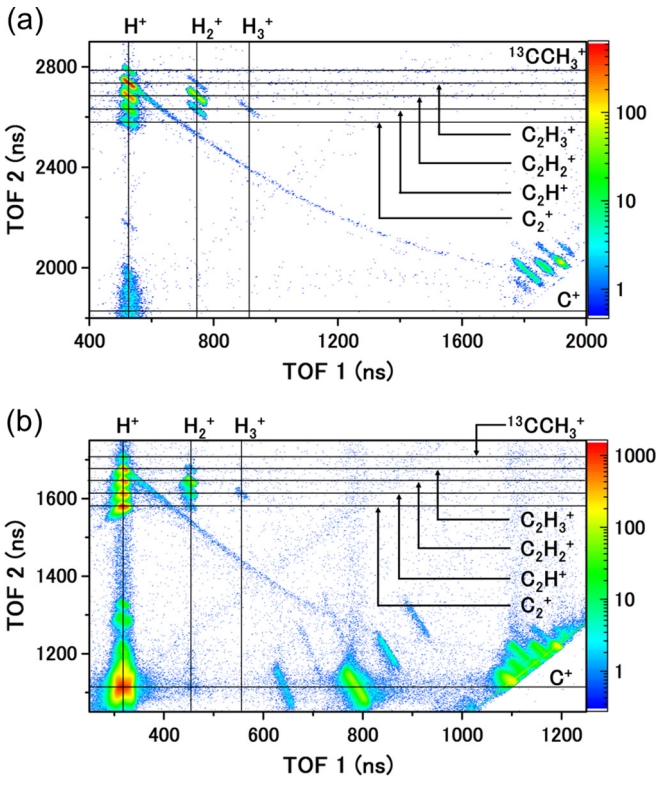

FIG. 2. Double-hit TOF coincidence maps for (a) 1.5 keV/u collision of Ar^{4+} triggered by an Ar^{3+} detection, and (b) that for 3.4 keV/u collision of Xe^{9+} triggered by an electron detection. The color indicates the intensity in the logarithmic scale. The vertical and horizontal lines indicate TOFs of the fragment ions without initial velocity components in the TOF axis. The diagonal line is due to the delayed dissociation.

of the experimental conditions is given. A schematic view of the TMU apparatus is shown in Fig. 1(a). Ethylene molecules were introduced into the beam-source chamber to form a gas jet. After trimming with a skimmer, the molecules drifted to the collision chamber and crossed the projectile beam. A liquid-nitrogen-cooled trap was used to terminate the jet. 1.5 keV/u Ar^{4+} and 3.0 keV/u Ar^{8+} were used as the projectiles. The recoil ions were accelerated in a *uniform* electric field (15.1 V/mm with a length of 204 mm). The PSTOF was measured in coincidence with the detection of the scattered Ar^{3+} or Ar^{2+} ions for Ar^{4+}, and Ar^{7+} or Ar^{6+} ions for Ar^{8+}, using a microchannel plate detector (MCP) with a capacitively coupled readout [22]. The pressure during operation was about 4×10^{-5} Pa while the background pressure was about 8×10^{-7} Pa. For each charge state of the scatter ions, 13–21 consecutive hours of data acquisition were performed.

Low- and medium-energy collision experiments were conducted at the beamline in the Low Energy Ion Beam Facility of the Inter-University Accelerator Centre (IUAC) [23], using Xe^{9+} beams with the energies of 3.4 and 17.0 keV/u. A schematic drawing of the IUAC apparatus is shown in Fig. 1(b). The target ethylene was introduced as an effusive beam, and the emitted electrons triggered the PSTOF measurement of the recoil ions. The recoil ions were collected with a *two-stage* extraction field (the first one with 52.8 V/mm, 18 mm, and the second one with 41.1 V/mm, 39 mm). After passing through the field free region (104.5 mm), the recoil ions are detected by a position- and time-sensitive detector (PSD) consisting of an MCP with a DLD anode [24]. The pressure during operation was about 1.9×10^{-5} Pa while the background pressure was about 6.3×10^{-6} Pa. Nineteen and fifteen consecutive hours of data acquisition were performed for 3.4 and 17 keV/u experiments, respectively.

III. RESULTS AND DISCUSSION

The PSTOF data recorded at TMU and IUAC were analyzed in detail, focusing attention onto the deprotonation events, which are identified in the double-hit coincidence map. The coincidence map for the charge-changing collision $Ar^{4+} \rightarrow Ar^{3+}$ is shown in Fig. 3(a). Hereafter the ionic dissociation channels will be denoted by (heavier fragment ion, lighter fragment ion), for example ($C_2H_3^+$, H^+) for the reaction (1).

In Fig. 2(a), the dissociation channels ($C_2H_3^+$, H^+) and ($C_2H_2^+$, H_2^+), due to 2-capture/1-Auger, are uniquely identified. The island of (C_2H^+, H_3^+) channel, which needs H atom migration, is weak but clearly above the background level.

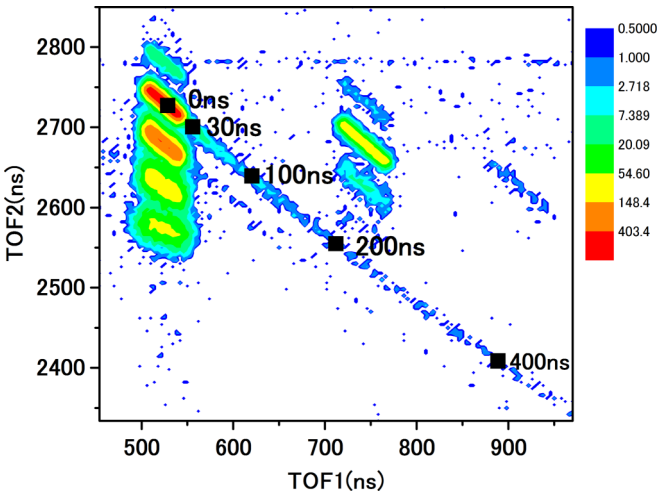

FIG. 3. Double-hit TOF coincidence map for 3.0 keV/u collision of Ar^{8+} with Ar^{7+} trigger, in expanded scale for ($C_2H_{4-n}^+$ (n = 1–4), H^+), ($C_2H_{4-n}^+$ (n = 2–4), H_2^+), and (C_2H^+, H_3^+) channels. The color indicates the intensity in logarithmic scale.

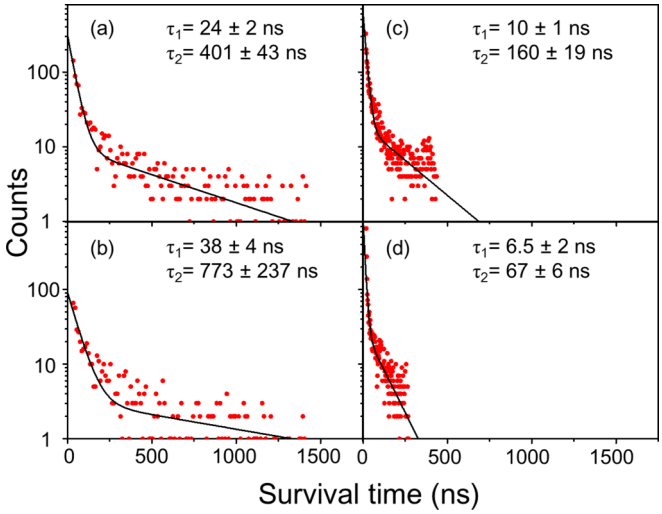

FIG. 4. Semilogarithmic histograms of the survival time of $C_2H_4^{2+}$ against delayed dissociation channel ($C_2H_3^+$, H^+), obtained for (a) 1.5 keV/u Ar^{4+}, (b) 3.0 keV/u Ar^{8+}, (c) 3.4 keV/u Xe^{9+}, and (d) 17.0 keV/u Xe^{9+}. The solid curves indicate fits by a two-component exponential function. The values of τ_1 and τ_2 with 1σ fitting uncertainty are shown in the figure. An additional slower component seems to be needed for better fit.

A long diagonal line, starting from the island ($C_2H_3^+$, H^+) and merging into the island (CH_2^+, CH_2^+), indicates delayed dissociation with a long survival time of the parent dication takes place. For ($C_2H_2^+$, H^+) channels, a less prominent profile of delayed reactions is also observed. Considering the slope of the profile, it is most likely due to the sequential reaction $C_2H_4^{2+} \rightarrow C_2H_3^{2+} + H \rightarrow C_2H_2^+ + H^+ + H$, where the second step is slow. Because of its low counts, the delayed process in the ($C_2H_2^+$, H^+) channel was not analyzed further. The coincidence map for $Ar^{8+} \rightarrow Ar^{7+}$ is similar whereas the island (CH_2^{2+}, CH^+) is observed because 3-capture/2-Auger occurs. The deprotonation channel in the true double capture events, namely those triggered by $Ar^{4+} \rightarrow Ar^{2+}$ and $Ar^{8+} \rightarrow Ar^{6+}$, was not analyzed because of low statistics.

A coincidence map for 3.4 keV/u Xe^{9+}, triggered by detection of an electron, is shown in Fig. 2(b). The ($C_2H_3^+$, H^+), ($C_2H_2^+$, H_2^+), and (C_2H^+, H_3^+) channels are due to 2-capture/1-Auger, namely they are equivalent to those for corresponding channels in Fig. 2(a), aside from the difference in the energies and the ionic species of the projectiles. Thus, it is not surprising that the (C_2H^+, H_3^+) channel and the delayed process of the ($C_2H_3^+$, H^+) channel are observed in Fig. 2(b). The coincidence map for 17.0 keV/u Xe^{9+} is similar to that in Fig. 2(b).

A coincidence map relevant to the delayed process is shown in Fig. 3, for collision of Ar^{8+} with Ar^{7+} trigger. As can be seen in the figure, the prompt dissociation is easily distinguishable. In the range TOF1 $\leqslant$ 560 ns ($\tau \leqslant$ 30 ns), the contribution of the direct dissociation becomes dominant. This area is excluded from subsequent analysis of the delayed process. The lifetimes of the transient $C_2H_4^{2+}$ are derived from the TOF shift from the prompt dissociation. That is, TOFs of H^+ (TOF1) and $C_2H_3^+$ (TOF2) are calculated as a function of the survival time τ of $C_2H_4^{2+}$, neglecting the KER of the delayed process, and then, τ for each event is obtained referring to the obtained function. Several calculated points in (TOF1, TOF2) coordinates are shown in Fig. 3. In the TOFs of the fragments, the kinetic energies of the dissociating fragment pair are convoluted. The uncertainty due to the energy spread is about 30 ns, negligible compared to the timescale of the survival times, as demonstrated in the prompt channel in Fig. 3. The same procedure is applied to the other collision systems, while the calculated function of the delayed profile is different between the data at TMU and IUAC, due to the difference in the experimental configurations. The cutoff of τ is set to be 16.5 ns for the IUAC data.

The histograms of the survival times, in semilogarithmic scale, are shown in Figs. 4(a)–4(d) for various collision systems. First they are fitted by double exponential functions, which gave a good fit in the previous laser study [16]. As indicated by the solid lines, all the decay profiles for shorter time ($\tau \leqslant$ 500 ns) are well fitted with double exponential functions, with the faster component $\tau_1 <$ 40 ns and slower component $\tau_2 \sim$ 60–800 ns. They might be different among the collision systems, whereas the fitting uncertainty is large. As demonstrated in (a) and (b), a better fit seems to be obtained by additional slower components. Even if the lifetime of 500 ns is adopted for the slower component as a restraint condition, which is the value obtained by the fs laser study [15], the overall feature cannot be well fitted.

Generally speaking, an exponential fit by more than two components leads to large tolerance, and a power-law fit offers an alternative. If the decaying ion has a broad energy distribution, and thus broad distribution of the rate constants, the log-log plot of the time and intensity gives a linear relation, indicating the validity of the power law [2–5]. The plots in Figs. 4(a)–4(d) are transformed to log-log plots, which commonly show a linear relation, with the slope (r) of near -1 as illustrated by the black lines in Figs. 5(a)–5(d). More accurately, $r = -1.2$ or -1.3 with a 1σ fitting uncertainty of

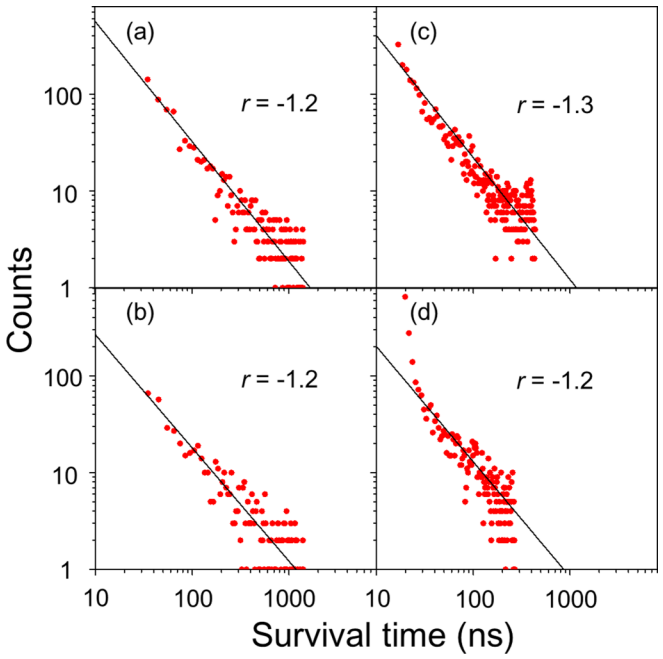

FIG. 5. Log-log plot of the histograms of the survival time of $C_2H_4^{2+}$ for (a) 1.5 keV/u Ar^{4+}, (b) 3.0 keV/u Ar^{8+}, (c) 3.4 keV/u Xe^{9+}, and (d) 17.0 keV/u Xe^{9+} (using the same data as in Fig. 4). The lines in black indicate the fitted functions of the power law decay (τ^r). The values of r are shown in the figures. In (d), a fast decay component is observed, which is ignored in the power-law fitting. Although the source of this component is not clear, it is likely due to insufficient exclusion of the prompt component.

0.02–0.04. Deviation of the power from $r = -1$ is observed for various ions undergoing evaporation of a *neutral* fragment. For example, $r = -0.9$ for bromouracil and glycine cations, and -1.1 for arginine cations [3,12]. The smaller (larger negative) r can be rationalized by taking account of the finite heat capacity of the ethylene molecule. The correction leads to $r = -1 - 1/(s - 1)$, where s is an effective number of degrees of freedom [2]. Probably the internal temperature of the dication is not very high, and s can be smaller than the value at the high temperature limit ($3N - 6 = 12$, corresponding to $t^{-1.1}$ dependence).

According to the previous laser study, theoretical lifetimes calculated for highly excited vibrational modes relevant to deprotonation (C-H stretching) are consistent with the experimental lifetime. Larimian *et al.* suggested that the vibronic state $^3A''(v = 8)$ and/or $^1A''(v = 10)$ directly populated by the Franck-Condon transition would be responsible for the delayed deprotonation. On the other hand, the power-law decay needs a large number of components with continuously varying rate constants. Such a requirement is fulfilled by assuming an indirect process, in which the intramolecular vibrational redistribution (IVR) is fast, namely the vibrational states (v) are statistically populated at a given total vibrational energy (E). Then, the decomposition rates of the small molecules, k_d, are given by the equation

$$k_d(E) = \sum_v k_{v,\text{tunnel}} \frac{\rho(E - E_v)}{\rho(E)}, \quad (1)$$

where $k_{v,\text{tunnel}}$ is the rate of the tunneling through the barrier at a specific vibrational state v of the relevant vibrational mode. E_v is the energy of this vibrational mode, and $\rho(E)$, $\rho(E - E_v)$ are the state density at E and that at the energy available for the rest of the modes. The factor $\rho(E - E_v)/\rho(E)$ is a continuously (and rapidly) changing function with E, giving rise to a broad distribution of $k_d(E)$ and the power-law decay. The numerical calculation of $k_d(E)$ is suspended at present, since reliable vibrational frequencies of the dication are needed for various electronic states. It should be stressed that, irrespective of the accurate shape of the $k_d(E)$ function, the power-law decay is rationalized as long as $k_d(E)$ varies continuously.

IV. SUMMARY

We have observed ionic dissociation induced by collisions of highly charged ions with energies from 1.5 to 17.0 keV/u, and found that the delayed dissociation of metastable $C_2H_4^{2+}$ is commonly well described by a power-law decay, indicating that dications with various internal energy contribute to the delayed formation of $C_2H_3^+ + H^+$ pairs with their characteristic rate constants. It also gives a reasonable interpretation of the fact that the decay profile does not much depend on the method of ionization.

ACKNOWLEDGMENTS

The authors would like to thank Dr. K. Hansen for his helpful comments relating the finite heat capacity correction. This work was supported by Japan Society for the Promotion of Science KAKENHI Grant No. JP15K05231. K.Y. is thankful for the support by the TMU travel fund.

[1] K. Hansen, *Statistical Physics of Nanoparticles in the Gas Phase* (Springer, Dordrecht, 2013).
[2] K. Hansen, J. U. Andersen, P. Hvelplund, S. P. Møller, U. V. Pedersen, and V. V. Petrunin, Phys. Rev. Lett. **87**, 123401 (2001).
[3] J. U. Andersen, H. Cederquist, J. S. Forster, B. A. Huber, P. Hvelplund, J. Jensen, B. Liu, B. Manil, L. Maunoury, S. B. Nielsen, U. V. Pedersen, H. T. Schmidt, S. Tomita, and H. Zettergren, Eur. Phys. J. D **25**, 139 (2003).
[4] J. U. Andersen, E. Bonderup, K. Hansen, P. Hvelplund, B. Liu, U. V. Pedersen, and S. Tomita, Eur. Phys. J. D **24**, 191 (2003).
[5] S. B. Nielsen, J. U. Andersen, P. Hvelplund, B. Liu, and S. Tomita, J. Phys. B: At. Mol. Opt. Phys. **37**, R25 (2004).
[6] C. P. Safvan and D. Mathur, J. Phys. B: At. Mol. Opt. Phys. **26**, L793 (1993).
[7] T. A. Field and J. H. D. Eland, Chem. Phys. Lett. **211**, 436 (1993).
[8] L. H. Andersen, J. H. Posthumus, O. Vahtras, H. Ågren, N. Elander, A. Nunez, A. Scrinzi, M. Natiello, and M. Larsson, Phys. Rev. Lett. **71**, 1812 (1993).
[9] D. Mathur, L. H. Andersen, P. Hvelplund, D. Kella, and C. P. Safvan, J. Phys. B: At. Mol. Opt. Phys. **28**, 3415 (1995).

[10] C. P. Safvan and D. Mathur, J. Phys. B: At. Mol. Opt. Phys. **27**, L477 (1994).
[11] J. Ma, H. Li, K. Lin, Q. Song, Q. Ji. W. Zhang, H. Li, F. Sun, J. Qiang, P. Lu, X. Gong, H. Zeng, and J. Wu, Phys. Rev. A **97**, 063407 (2018).
[12] R. Delaunay, J.-P. Champeaux, S. Maclot, M. Capron, A. Domaracka, A. Méry, B. Manil, L. Adoui, P. Rousseau, P. Moretto-Capelle, and B. A. Huber, Eur. Phys. J. D **68**, 162 (2014).
[13] S. Tomita, H. Lebius, A. Brenac, F. Chandezon, and B. A. Huber, Phys. Rev. A **67**, 063204 (2003).
[14] B. Gaire, S. Y. Lee, D. J. Haxton, P. M. Pelz, I. Bocharova, F. P. Sturm, N. Gehrken, M. Honig, M. Pitzer, D. Metz, H.-K. Kim, M. Schöffler, R. Dörner, H. Gassert, S. Zeller, J. Voigtsberger, W. Cao, M. Zohrabi, J. Williams, A. Gatton, D. Reedy, C. Nook, Thomas Müller, A. L. Landers, C. L. Cocke, I. Ben-Itzhak, T. Jahnke, A. Belkacem, and Th. Weber, Phys. Rev. A **89**, 013403 (2014).
[15] S. Larimian, S. Erattupuzha, E. Lötstedt, T. Szidarovszky, R. Maurer, S. Roither, M. Schöffler, D. Kartashov, A. Baltuška, K. Yamanouchi, M. Kitzler, and X. Xie, Phys. Rev. A **93**, 053405 (2016).
[16] B. Jochim, R. Erdwien, Y. Malakar, T. Severt, B. Berry, P. Feizollah, J. Rajput, B. Kaderiya, W. L. Pearson, K. D. Carnes, A. Rudenko, and I. Ben-Itzhak, New J. Phys. **19**, 103006 (2017).
[17] I. Bocharova, R. Karimi, E. F. Penka, J.-P. Brichta, P. Lassonde, X. Fu, J.-C. Kieffer, A. D. Bandrauk, I. Litvinyuk, J. Sanderson, and F. Légaré, Phys. Rev. Lett. **107**, 063201 (2011).
[18] H. Tanuma, J. Matsumoto, T. Nishide, H. Shiromaru, and N. Kobayashi, J. Chin. Chem. Soc. **48**, 389 (2001).
[19] K. Hayakawa, J. Mastumoto, H. Shiromaru, and Y. Achiba, J. Phys. B: At. Mol. Opt. Phys. **44**, 075207 (2011).
[20] J. Matsumoto, K. Nakadai, T. Motojima, Y. Achiba, and H. Shiromaru, J. Phys.: Conf. Ser. **388**, 102058 (2012).
[21] J. Matsumoto, H. Tezuka, and H. Shiromaru, J. Phys.: Conf. Ser. **583**, 012016 (2015).
[22] T. Mizogawa, H. Shiromaru, M. Sato, and Y. Itoh, Int. J. Mass Spectrom. Ion Phys. **215**, 141 (2002).
[23] A. Kumar, J. Rajput, T. Sairam, M. R. Jana, L. Nair, and C. P. Safvan, Int. J. Mass Spectrom. **374**, 44 (2014).
[24] O. Jagutzki, V. Mergel, K. Ullmann-Pfleger, L. Spielberger, U. Meyer, R. Dörner, and H. Schmidt-Böcking, Proc. SPIE **3438**, 322 (1998).